Tidal Heating via Internal Gravity Waves in White Dwarf Binaries

Authors
(Dated: January 14, 2019)

In white dwarf binaries tidal torques are expected to raise a train of internal gravity waves in the white dwarf interior. These outward-propagating waves can then grow to be nonlinear and break via hydrodynamical instabilities, transfering energy and angular momentum from the binary orbit to the white dwarf. We perform 2D numerical simulations of nonlinear wave breaking of outwards-propagating internal gravity waves in an incompressible, isothermal atmosphere with an exponentially decaying density stratification. We find that tidal synchronization, after an initial transient phase, proceeds inwards from the surface in thin layers. We argue the thickness of these layers is limited by the Kelvin-Helmholtz Instability. We provide simple analytical formulae for the location and thickness of tidal synchronization over time that are in good agreement with our simulations.

I. INTRODUCTION

In §II, we will cover the numerical setup. In §III, we will discuss the agreement of our simulation in the low-amplitude limit with analytical linear theory. In §IV we will present a few reference simulations illustrating critical layer absorption depositing horizontal angular momentum into the fluid.

II. PROBLEM DESCRIPTION

A. Fluid Equations

We consider an incompressible, isothermal fluid, representative of degenerate matter in WD bulks, in 2D. We assume a barotropic equation of state as a first approximation. As we are interested in the behavior of the wave far from the center of the WD, we approximate the gravitational field as uniform. We model the background density stratification as $\rho_0(x,z) = \rho_0(z) = \rho_{ref}e^{-z/H}$ for some reference density $\rho_{ref} = \rho_0(z)|_{z=0}$.

The Euler equations for an incompressible, barotropic fluid in a uniform gravitational field are

$$\vec{\nabla} \cdot \vec{u} = 0, \tag{1a}$$

$$\frac{\mathrm{D}\rho}{\mathrm{D}t} = 0, \tag{1b}$$

$$\frac{\mathrm{D}\vec{u}}{\mathrm{D}t} + \frac{\vec{\nabla}P}{\rho} + g\hat{z} = 0. \tag{1c}$$

$\frac{\mathrm{D}}{\mathrm{D}t} = \frac{\partial}{\partial t} + \left(\vec{u} \cdot \vec{\nabla}\right)$ is the material derivative. $\vec{u}, \rho, P$ are the fluid dynamical variables and $-g\hat{z}$ is constant gravitational acceleration. Note that at hydrostatic equilibrium $\frac{\partial}{\partial t} = 0$ we have $\vec{\nabla}P_0 = -\rho_0 g\hat{z}$ and so $P_0 = \rho_0 gH$. A shear flow $u_x(x,z,t) = u_x(z)$ is permitted in hydrostatic equilibrium, but we will initially consider no shear flow in equilibrium.

B. Internal Gravity Waves: Linear Theory

In the small perturbation limit, where flow velocities are small compared to the characteristic space and time scales $\frac{\partial}{\partial t} \gg \vec{u} \cdot \vec{\nabla}$, we linearize Eq. 1 by ignoring the advective components of the material derivative, defining $\rho_1 \equiv \rho - \rho_0 \ll \rho_0$ and $P_1 \equiv P - P_0$ deviations from equilibrium and obtain:

$$\vec{\nabla} \cdot \vec{u} = 0, \tag{2a}$$

$$\frac{\partial \rho_1}{\partial t} - \frac{u_z \rho_0}{H} = 0, \tag{2b}$$

$$\frac{\partial \vec{u}}{\partial t} + \frac{\vec{\nabla}P_1}{\rho_0} + \frac{\rho_1 g\hat{z}}{\rho_0} = 0. \tag{2c}$$

It is well known that the solutions to the $F = 0$ homogeneous Eq. 2 are of form (cite)

$$u_z(x,z,t) = Ae^{z/2H}e^{i(k_{0x}x + k_{0z}z - \omega_0 t)}, \tag{3a}$$

$$\omega_0^2 = \frac{N^2 k_{0x}^2}{k_{0x}^2 + k_{0z}^2 + \frac{1}{4H^2}}, \tag{3b}$$

up to undetermined amplitude A, where

$$N^2 \equiv g^2\left(\frac{\mathrm{d}\rho}{\mathrm{d}P} - \frac{\partial \rho}{\partial P}\bigg|_{ad}\right) = \frac{g}{H}, \tag{4}$$

is the Brunt-Väisälä, or buoyancy, frequency.

In the weak stratification limit $k_z H \gg 1$, the solution exhibits the following characteristics:

- The amplitude of the perturbations grows like $e^{z/2H}$. Thus, the linear approximation is violated for sufficiently large z.

- The phase and group velocities can be computed

respectively:

$$\vec{c}_{ph} = \frac{Nk_x}{k_x^2 + k_z^2 + 1/4H^2}\hat{k}, \tag{5}$$

$$\vec{c}_g = \frac{N\left(k_x k_z \hat{x} - \left(k_z^2 + \frac{1}{4H^2}\right)\hat{z}\right)}{\left(k_x^2 + k_z^2 + \frac{1}{4H^2}\right)^{3/2}}$$

$$\approx \frac{Nk_z}{k_x^2 + k_z^2}(k_x \hat{x} - k_z \hat{z}). \tag{6}$$

We recover the usual result $\vec{c}_{ph} \cdot \vec{c}_g = 0$ (CITE). Note that an IGW transporting energy and momentum upwards has $k_z < 0$.

- The time-averaged total x-momentum flux in the $\hat{z}$ direction can be computed. Since the fluid variables have separable as $f(x,z,t) = f(z)e^{i(k_{0x}x - \omega_0 t)}$, x averaging and time averaging are equivalent, so we may write ($\langle \ldots \rangle_x$ denotes x-averaging)

$$F_{px,z} \equiv \langle \rho u_x u_z \rangle_x = \frac{1}{L_x}\int_0^{L_x} \rho u_x u_z \, dx$$

$$\approx -\frac{A^2}{2}\rho_{ref}\frac{k_z}{k_x}. \tag{7}$$

- Finally, it may be noted that horizontally averaged horizontal momentum $p_x = \langle \rho u_x \rangle_x$ obeys $\frac{\partial p_x}{\partial t} + \frac{\partial F_{px}}{\partial z} = 0$. Since flux is transported on the group velocity timescale (CITE), this simplifies to the known expression for the wave-induced horizontal mean flow (cite)

$$\bar{U}_0 \equiv \langle u_x \rangle_x = \frac{\langle u_x u_z \rangle_x}{c_{gz}} \tag{8}$$

We've denoted $c_{gz} = \left.\frac{\partial \omega}{\partial k_z}\right|_{k_{z0}}$ the vertical group velocity. In terms of our forcing amplitude,

$$\bar{U}_0(F) = -\frac{A(F)^2}{2}e^{\frac{z-z_0}{H}}\frac{k_z}{k_x}c_{gz}, \tag{9}$$

where $c_{gz} = -\frac{Nk_{0x}k_{0z}}{\left(k_{0x}^2 + k_{0z}^2 + \frac{1}{4H^2}\right)^{3/2}}$.

C. Wave Generation

To model a continuous IGW wave train excited deep in the WD interior propagating towards the surface without unnecessary computational cost, we excite an IGW wave train from the bottom of the simulation domain. We use a volumetric forcing term to excite IGW at some $z_0 > 0$ interior to the simulation domain[1]. Our forc-

ing excites both IGWs propagating upwards, imitating a wave tidally excited deeper in the WD, and downwards, which are damped away by damping layers (see §II D) before inducing strict Courant-Friedrichs-Lewy (CFL) timestepping constraints.

As not to interfere with the incompressibility constraint, we force the system on the density equation, replacing Eq. 1b with

$$\frac{D\rho}{Dt} = Fe^{-\frac{(z-z_0)^2}{2\sigma^2}}\cos(k_{0x}x - \omega_0 t). \tag{10}$$

Using a narrow Gaussian profile excites a broad k_z wavenumber spectrum, and only the k_{0z} satisfying the IGW's dispersion relation for the given $k_{0x}, \omega_0(k_{0x}, k_{0z})$ will propagate. The fluid equations then take form

$$\vec{\nabla} \cdot \vec{u} = 0, \tag{11a}$$

$$\frac{D\rho}{Dt} = Fe^{-\frac{(z-z_0)^2}{2\sigma^2}}e^{i(k_x x - \omega t)}, \tag{11b}$$

$$\frac{D\vec{u}}{Dt} + \frac{\vec{\nabla}P}{\rho} + g\hat{z} = 0. \tag{11c}$$

The linearized Eq. 11, obtained by dropping the advective term in the material derivative, can be solved analytically up to good accuracy. We may first approximate the driving term using $e^{\frac{-(z-z_0)^2}{2\sigma^2}} \approx \sqrt{2\pi\sigma^2}\delta(z-z_0)$ if $\sigma \to 0$[2]. This system is solved exactly by matching the two homogeneous solutions above and below z_0, We may then approximately relax the solution to $k_{0z}\sigma \lesssim 1$: an extra factor of $e^{-\frac{(k_{0z}\sigma)^2}{2}}$ arises compared to the δ-function solution (evaluating the Fourier Transform of $e^{-\frac{(z-z_0)^2}{2\sigma^2}}$ at $k_z = k_{0z}$), and we obtain

$$A(F) = \frac{Fgk_{0x}^2}{\rho_0(z_0)\omega_0^2}\frac{1}{2ik_z}\frac{e^{\frac{-(k_{0z}\sigma)^2}{2}}}{\sqrt{2\pi\sigma^2}}, \tag{12}$$

$$u_{1z}(x,z,t) = A(F)\times$$

$$\begin{cases} e^{\frac{z-z_0}{2H}}e^{i(k_{0x}x + k_{0z}(z-z_0) - \omega_0 t)} & z > z_0 \\ e^{\frac{z-z_0}{2H}}e^{i(k_{0x}x - k_{0z}(z-z_0) - \omega_0 t)} & z < z_0 \end{cases}. \tag{13}$$

D. Numerical Parameters

We nondimensionalize by taking $H = N = \rho_{ref} = 1$

---

[1] Interfacial forcing at the bottom boundary incurs severe CFL timestepping constraints, as we use a Chebyshev polynomial basis along the z axis in our spectral method which has very small grid spacing at the boundaries.

[2] σ must be large enough to be numerically resolved by the spectral code.

These are implemented as:

$$\vec{\nabla} \cdot \vec{u} = 0, \tag{14a}$$

$$\frac{\partial \Upsilon}{\partial t} - \frac{u_z}{H} - \nu \nabla^2 \Upsilon = -\Gamma(z)\Upsilon - \left(\vec{u} \cdot \vec{\nabla}\right)\Upsilon + \frac{F}{\rho_0(z)} \cos(k_z z) \tag{14b}$$

$$\frac{\partial u_x}{\partial t} + \frac{\partial T}{\partial x} + gH\frac{\partial \Upsilon}{\partial x} - \nu \nabla^2 u_x = -\Gamma(z)u_x - \left(\vec{u} \cdot \vec{\nabla}\right)u_x - T_1 \frac{\partial \Upsilon}{\partial x}, \tag{14c}$$

$$\frac{\partial u_z}{\partial t} + \frac{\partial T}{\partial z} + gH\frac{\partial \Upsilon}{\partial z} - \frac{T_1}{H} - \nu \nabla^2 u_z = -\Gamma(z)u_z - \left(\vec{u} \cdot \vec{\nabla}\right)u_z - T_1 \frac{\partial \Upsilon}{\partial z} \tag{14d}$$

$$\Gamma(z) = 7.5\left[2 + \tanh\frac{z - z_T}{(L_z - z_T)/2} + \tanh\frac{z_B - z}{z_B/2}\right] \tag{14e}$$

where $z_B = 0.05L_z$, $z_T = 0.95L_z$ are the boundaries of the damping zones. A Navier-Stokes numerical viscosity ν is used to damp high wavenumbers and regularize the nonlinear cascade at near grid resolution: $\nu \sim 0.2\frac{\omega}{|k_z|}\frac{L_z}{2\pi N_z}$ was found to be suitable for $N_z = 1024$, where k_z is the wavenumber of the excited linear mode.

The exact implementation of these equations in Dedalus is described in §A.

III. LINEAR REGIME

We first test our numerical simulation with a "linear" simulation, where all flow quantities are small: we assume $\rho_1 \equiv \rho - \rho_0 \ll \rho_0$ and $\vec{u} \cdot \vec{\nabla} \ll \partial_t$. We emphasize that our "linear" simulations solve the full nonlinear equations, just in the weak perturbation limit.

ω is chosen by inverting $\omega(k_x, k_z)$ dispersion relation for fixed $k_x = 2\pi/L_x$ and some desired $k_z = -2\pi/H$, and $\sigma \lesssim \frac{1}{k_z}$ is used to excite a broad band of modes including the desired k_z mode.

A. Numerical Simulation

We simulate using Dedalus (cite) a spectral numerical method. We use a Fourier basis in the x direction and a Chebyshev in the z direction. Our simulation starts with all perturbation quantities at zero, an initial condition at rest. Our parameters are chosen to be as similar as possible to the later nonlinear simulations (§IV). We choose as follows:

- k_{0x}: Astrophysical IGWs have $k_x \ll k_z$, so we choose $k_{0x} = \frac{2\pi}{L_x}$ the smallest permitted wavenumber permitted by periodic boundary conditions.

- We choose ω_0 by choosing it to produce a desired k_{0z}. Astrophysical systems generally also exhibit $k_z H \gg 1$, where the stratification height is significantly larger than the vertical wavelength.

However, in order for the simulation to both be well-damped at grid resolutions and be neglibily damped at leading order nonlinear wavelengths, we require $k_{0z} \ll \frac{1}{L_{NL}} \ll \frac{2\pi N_z}{L_z}$, where L_{NL} denotes some characteristic length scale of nonlinear features. Finally, we need L_z to be many H to capture significant $e^{z/2H}$ growth and separate the linear and nonlinear amplitudes of u_z.

Fixing $L_z = 10H$ to give $\sim e^4$ amplitude growth between the damping zones, this implies we require separation of scales $1 \ll k_{0z}H \ll \frac{H}{L_{NL}} \ll \frac{2\pi N_z}{10}$.

Since N_z is fixed by computational cost (we tried both $N_z \equiv 512$, $N_z = 1024$), we choose $k_{0z} \sim \frac{2\pi}{H}$. This is less physically representative but gives more wavenumber space for the nonlinear cascade. We then invert $\omega_0 = \omega(k_{0x}, k_{0z})$.

- We choose ν 1/10 that of the nonlinear simulation, to verify that the undamped linear solution is recovered.

- We choose F forcing strength 1/20 that of the nonlinear simulation, which keeps the flow amplitude sufficiently small to be treated in the linear approximation at all points in the simulation domain.

A representative snapshot of this simulation is provided in Fig. 1. Key features to note:

- u_z grows with Eq. 13 to reasonable accuracy.

- F_{px} is seen to be constant, as would be expected by Eq. 7.

- $\bar{U}_0$ agrees with Eq. 9 at lower z but deviates significantly at higher z. This deviation is caused by the top damping zone that does not conserve horizontal momentum.

We also include a qualitatively similar snapshot of the same simulation run using the ν from the later nonlinear simulations in Fig. 2.

IV. NONLINEAR REGIME

A. Mean Flow Critical Layer Absorption

In past studies of IGWs in WDs (cite Fuller & Lai), $\xi_z \equiv \frac{u_z}{\omega_0}$ the Lagrangian fluid displacement was often used towards wave breaking criterion $k_{0z}\xi_z \gtrsim 1$. We argue that the wave's self-interaction via its generated mean flow $\bar{U}_0$ induces total absorption when the mean flow exceeds critical value

$$\bar{U}_c = \frac{\omega_0}{k_{0x}}. \tag{15}$$

This is consistent with the picture put forth in e.g. Goldreich and Nicholson (cite).
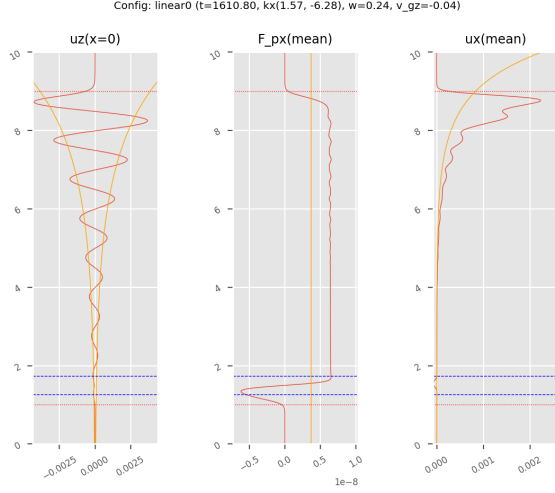
FIG. 1: Snapshot of linear simulation after reaching steady state. Analytical predictions of $|u_z|, \bar{U}_0, F_{px}$ are shown in orange. Red dotted lines indicate the onset of the damping region and blue dotted lines denote the driving region.
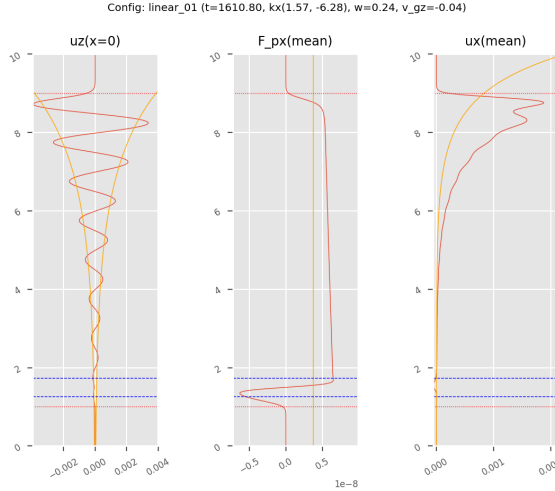

FIG. 2: Same as Fig. 1 but with $0.3\times$ viscosity used for nonlinear simulations (YUBONOTE should be the same but that simulation mysteriously stopped without me noticing; restarting worked, so currently rerunning). Note the slight resulting dissipation in F_{px}.

A purely horizontal shear flow $\bar{U}_0(z)\hat{x}$ can be seen in Eq. 1 to have the effect of modifying time derivatives ∂_t to their frequency in the comoving frame of the fluid $\partial_t - \bar{U}_0(z)\partial_x$. For a critical value $\omega_0 - \bar{U}_c k_{0x} = 0$, the frequency of the linear wave in the fluid's frame of reference vanishes and critical behavior is observed. In a linear theory or a theory where small scales are viscosity rather than advection dominated, the incident wave has amplitude reflection and transmission coefficients

$$\mathcal{R} = e^{-2\pi\sqrt{\mathrm{Ri}-\frac{1}{4}}}, \qquad \mathcal{T} = e^{-\pi\sqrt{\mathrm{Ri}-\frac{1}{4}}}, \qquad (16)$$

where we have defined Richardson number $\mathrm{Ri} \equiv$

$$\left.\frac{N^2}{\left(\frac{\partial \bar{U}_0}{\partial z}\right)^2}\right|_{z_c} \quad \text{at the critical layer } z_c : \bar{U}_0(z_c) = \frac{\omega_0}{k_{0x}}. \text{ For}$$

most shear flows, $\mathrm{Ri} \gg 1$ and so $\mathcal{R}, \mathcal{T} \ll 1$ and the incident wave is absorbed.

When the fluid absorbs the incident wave, it absorbs the incident horizontal momentum flux as well, which is converted into additional horizontal momentum of the shear flow. Since the shear flow cannot exceed $\bar{U}_c$ the horizontal phase velocity of the incident wave, the critical layer must thus propagate downwards (towards the wave source) to accommodate the incident momentum. In other words, the total horizontal momentum of the shear flow obeys conservation equation

$$\frac{\partial}{\partial t}\int_0^{L_z} \rho(z)\bar{U}_0(z,t)\,\mathrm{d}z - F_{px} = 0. \qquad (17)$$

Treating $\bar{U}_0(z > z_c) = \bar{U}_c, \bar{U}(z < z_c) = 0$ gives us exactly

$$\rho\bar{U}_c\frac{\partial z_c}{\partial t} = -F_{px}. \qquad (18)$$

B. Numerical Simulation

We use the same k_{0x}, ω_0 as §III A. Our other parameters are:

- We choose $\nu = 0.35\frac{\omega_0}{k_{0z}k_{z,\max}}$, where $k_{z,\max} = \frac{2\pi N_z}{L_z}$. Note that $\nu = \frac{\omega_0}{k_{0z}k_{z,\max}}$ corresponds to the advective term $\vec{u}\cdot\vec{\nabla}$ being of the same order as the time derivative ∂_t for flow velocities $\vec{u} \sim \frac{\omega_0}{k_{0z}}$ at the grid spacing.

- We choose F such that $\bar{U}_0(z)$ predicted by Eq. 9 exceeds $\bar{U}_c$ critical velocity for $z < L_z$, i.e. the wave-induced mean flow is sufficiently large within the simulation domain to induce critical layer absorption.

Two representative snapshots from our simulation are provided in Fig. 3 after the critical layer has had time to form. We may note that the critical layer, where F_{px} is absorbed and $\bar{U}_0 = \bar{U}_c$, travels downwards as predicted.

C. Propagating Critical Layer

For the simulation in Fig. 3, we may define $z_c = \mathrm{argmax}_z \frac{\partial \bar{U}_0}{\partial z}$. Computing $\frac{\partial z_c}{\partial t}$ using the analytical flux Eq. 7 allows comparison to Eq. 18, which we exhibit in Fig. 4. We see overall good agreement, though some small deviation is expected since F_{px} is not perfectly conserved owing to numerical viscosity (and YUBONOTE F_{px} is misestimated?).

However, recalling Eq. 16, we only expect complete critical layer absorption when $\mathrm{Ri} \gg \frac{1}{4}$. We may plot Ri
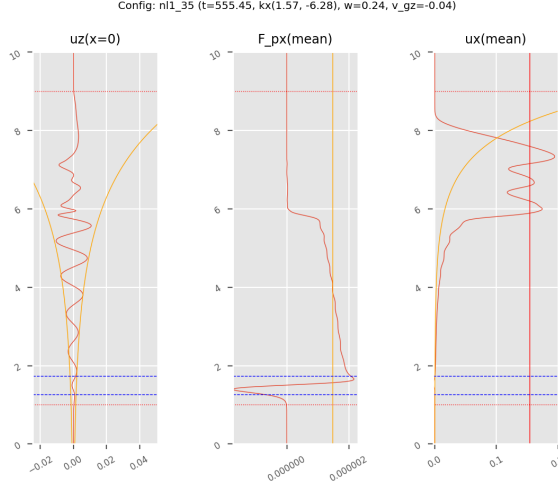
(a) Earlier time snapshot. Legend is the same as Fig. 1 except $\bar{U}_c$ is marked in red on the third panel.
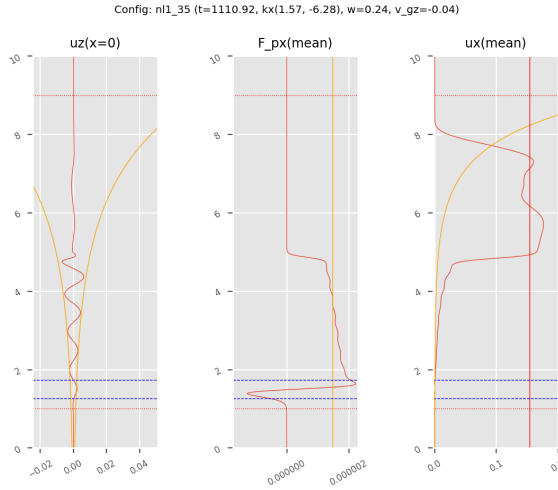
(b) Later snapshot illustrating propagation of z_c.
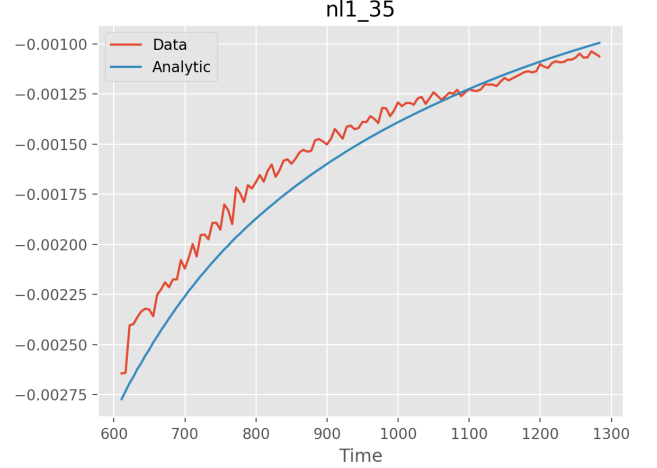
FIG. 3: Nonlinear numerical simulation.

FIG. 4: Comparison of simulated $\frac{\partial z_c}{\partial t}$ to analytical Eq. 18. Plot begins after formation of critical layer in simulation.
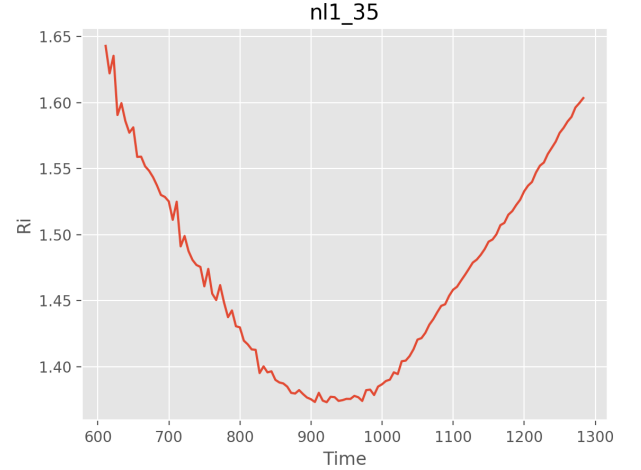

FIG. 5: Plot of $\mathrm{Ri}_{\max}(t) = \max_z \frac{N^2}{\bar{U}_0'}(t)$ over the simulation time.

over the same time interval in Fig. 5. We may observe that the Richardson number is initially decreasing but eventually levels out and begins to increase again. This corresponds to an increasingly sharp critical layer transition then subsequently a decreasingly sharp critical layer transition.

We argue that the Richardson number is bounded from below by viscosity. A repeated simulation with a larger viscosity is shown in Fig. 6, where the Richardson number does not go nearly as low.

Additionally, a lower-viscosity simulation shows significant features resembling Kelvin-Helmholtz instabilities (KHI), Fig. 7. As we have only plotted $\bar{U}_0(z)$, the local Richardson number $N^2/\frac{\partial u_x}{\partial z}$ may exceed the plotted value and incur KHIs.

This seems to suggest that our reference simulation is viscosity limited. This is perhaps physical: a Richardson number ~ 0.25 incurs the KHI which saps energy and angular momentum from the flow. It is conceivable then that our numerical viscosity is physically motivated as a effective KHI viscosity.

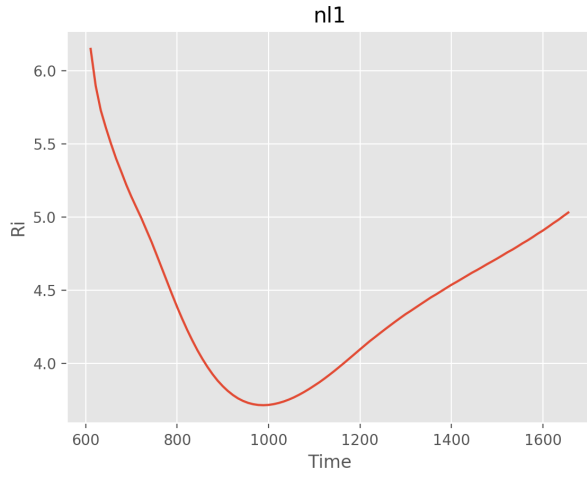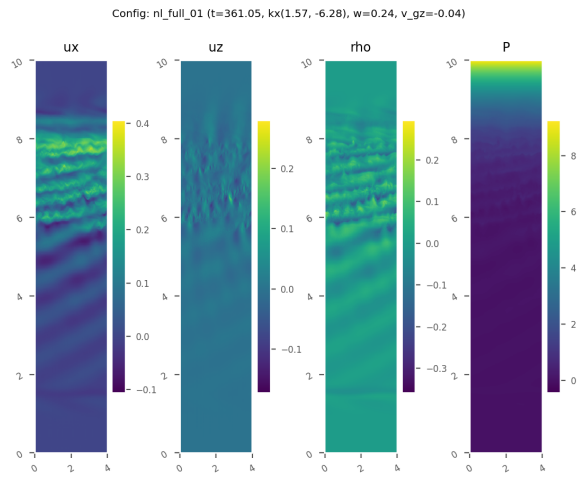**FIG. 6:** Same as Fig. 5 but with $\sim 1.3\times$ viscosity.

FIG. 7: Low viscosity simulation showing seemingly KHI-like features.

Appendix A: Equation Implementations

We denote $x \in [0, L_x]$, $z \in [0, L_z]$ the simulation domain and N_x, N_z the number of spectral modes in the respective dimensions. We perform direct numerical simulation of Eq. 11 with the open-source pseudo-spectral code Dedalus (CITE).

Numerically, the nonlinear $\frac{\vec{\nabla} P}{\rho}$ term is problematic: we desire a system where the fluid fields are not divided by one another. We introduce $\varpi = \frac{P}{\rho}$ instead, then mandate ρ_0, ϖ_0 background fields satisfy hydrostatic equilibrium $\vec{\nabla} \varpi_0 + \varpi_0 \vec{\nabla} \rho_0 + g \hat{z} = 0$. Taking isothermal stratification, we find $\varpi_0 = gH$. We further change variables to $\Upsilon = \ln \rho - \ln \rho_0$ and $\varpi_1 = \varpi - \varpi_0$ deviations from the background state to obtain a system of equations at most quadratic in fluid fields:

$$\vec{\nabla} \cdot \vec{u} = 0, \tag{A1a}$$

$$\frac{\partial \Upsilon}{\partial t} + \left(\vec{u} \cdot \vec{\nabla} \right) \Upsilon - \frac{u_z}{H} = 0, \tag{A1b}$$

$$\frac{\partial u_x}{\partial t} + \left(\vec{u} \cdot \vec{\nabla} \right) u_x + \frac{\partial \varpi_1}{\partial x} + gH \frac{\partial \Upsilon}{\partial x} + \varpi_1 \frac{\partial \Upsilon}{\partial x} = 0, \tag{A1c}$$

$$\frac{\partial u_z}{\partial t} + \left(\vec{u} \cdot \vec{\nabla} \right) u_z + \frac{\partial \varpi_1}{\partial z} + gH \frac{\partial \Upsilon}{\partial z} + \varpi_1 \frac{\partial \Upsilon}{\partial z} - \frac{\varpi_1}{H} = 0. \tag{A1d}$$

It bears noting that these equations are exactly equivalent to the original Euler equations and hence conserve horizontal momentum.

1. Artificial Dissipation

The nonlinear terms in the above equations will transfer energy from lower wavenumbers to higher wavenumbers. Since spectral codes have no numerical dissipation, artificial dissipation must be added. To ensure the dissipitive system conserves horizontal momentum, we begin by adding dissipitive terms to the flux-conservative form of the Euler fluid equations Eq. 1 (we use stress tensor $\tau_{ij} = P \delta_{ij}$):

$$\vec{\nabla} \cdot \vec{u} = 0, \tag{A2a}$$

$$\partial_t \rho + \vec{\nabla} \cdot (\rho \vec{u} - \nu \vec{\nabla} (\rho - \rho_0)) = 0, \tag{A2b}$$

$$\partial_t (\rho \vec{u}) + \vec{\nabla} \cdot (\rho \vec{u} \vec{u} + \mathrm{diag}(\rho \varpi) - \nu \rho \vec{\nabla} \vec{u}) + \rho g \hat{z} = 0. \tag{A2c}$$

The same ν is used for both the diffusive and viscous term, though this is not required. Since the dissipation is not physical and is purely used for numerical stability, we choose it such that hydrostatic equilibrium is not modified. Some algebraic manipulation to re-cast it in the form of Eq. A1 gives

$$\vec{\nabla} \cdot \vec{u} = 0, \tag{A3a}$$

$$\partial_t \Upsilon + \left(\vec{u} \cdot \vec{\nabla} \right) \Upsilon - \frac{u_z}{H} - \nu \left(\nabla^2 \Upsilon + \left(\vec{\nabla} \Upsilon \right) \cdot \left(\vec{\nabla} \Upsilon \right) - \frac{2}{H} \partial_z \Upsilon + \frac{1 - e^{-\Upsilon}}{H^2} \right) = 0, \tag{A3b}$$

$$\partial_t \vec{u} + \left(\vec{u} \cdot \vec{\nabla} \right) \vec{u} + \vec{\nabla} \varpi + \varpi \vec{\nabla} \Upsilon - \nu \nabla^2 \vec{u} + \vec{u} \nu \left(\nabla^2 \Upsilon + \left(\vec{\nabla} \Upsilon \right) \cdot \left(\vec{\nabla} \Upsilon \right) - \frac{2}{H} \partial_z \Upsilon + \frac{1 - e^{-\Upsilon}}{H^2} \right)$$
$$- 2\nu \left(\left(\left(\vec{\nabla} \Upsilon \right) \cdot \vec{\nabla} \right) \vec{u} - \frac{1}{H} \partial_z \vec{u} \right) - \frac{\varpi_1}{H} = 0. \tag{A3c}$$

Hydrostatic equilibrium is still $\vec{\nabla} \varpi_0 + g \hat{z} = 0$ where $\rho = \rho_0$, $\vec{u} = 0$. Including the damping layers and forcing terms as described in §II D, we finally obtain the full system of equations as simulated in Dedalus: